Arch. Metall. Mater. **67** (2022), 1, 105-111

DOI: https://doi.org/10.24425/amm.2022.137478

HAMID SAZEGARAN[1*], HASAN BAHARI[1], ALI MOHAMMAD NASERIAN-NIK[2], FARHAD KHORRAMSHAHI[3]

THE INFLUENCE OF ALUMINUM CONTENT ON THE POROSITY, MICROSTRUCTURE, AND MECHANICAL PROPERTIES OF POWDER METALLURGY STEELS

An experimental study was performed to assess the influences of aluminum content on the porosity, microstructure and mechanical properties of powder metallurgy steels. Optical microscope equipped with the image processing software and the scanning electron microscope were employed to study the microstructure of investigated specimens. In order to find mechanical properties of specimens, Vickers hardness and compression tests were conducted. By increasing the aluminum content (from 0 to 4 wt. %), the porosity increases (from 6.01% to 8.43%). The microstructure of specimens contains aluminum phase distributed between the boundaries of agglomerated iron particles, ferrite, and pearlite. By increasing the aluminum content, stress-strain curves shift significantly downwards, and the modulus of elasticity, elongation, yield stress, and Vickers hardness reduce from 1.82 to 0.86 GPa, 32.1 to 17.8%, 138.1 to 28.2 MPa, and 127.7 to 26.8 HV, respectively.

Keywords: aluminum content; powder metallurgy steel; porosity; microstructure; mechanical properties

1. Introduction

In recent years, sintered iron-carbon steels manufactured through powder metallurgy (PM) have been successfully replaced by ferrous alloys manufactured by other processes such as: casting and forming [1-4]. The powder metallurgy route involves the preparing and blending of powders, compaction, sintering, and finishing operations [5,6]. The most important features of the powder metallurgy process are: low cost, low waste of materials and low energy consumption, high surface quality and high dimensional accuracy, controlled density and porosity, high manufacturing rate and also wide variations in compositions. The properties of PM components depend significantly on the composition of powders' mixture, powder properties (shape and size, and distribution of particles), additives and lubricants, as well as compacting pressure, sintering temperature, time, and atmosphere, and cooling rate after sintering [7-10]. The mechanical properties of PM steels are strongly influenced by the processing factors, alloying elements, sintering conditions, and the porosity [11,12]. It was found that high amounts of porosity reduce the mechanical properties of PM steels by initiating the micro-cracks, accelerating the growth of micro-cracks, and increasing the stress concentration [13-15]. To strengthen the PM steels, the proper heat treatment, controlling the cooling rate after sintering and the appropriate amounts of additional alloying elements such as: Cu, P, Cr, Mo, Ni, Mn and Al can be applied [16-19]. The proper alloying elements can affect the microstructure and porosity (pore size, shape, and distribution) of PM steels, and as a result, can influence the mechanical properties [20].

The addition of carbon in the PM steels increases formation of the equilibrium liquid phase during sintering and results in the improvement of its densification [21-23]. In addition, carbon strongly affects the formation of pearlite layers and microstructure [24]. The PM steels with higher carbon contents require longer times for reactivity, dissolution and diffusion of carbon and pearlite formation during the sintering [25]. Boron, due to formation of the borides and the borocarbides, is an effective element for facilitating sintering process. This element significantly decreases the porosity of PM steels due to eutectic reaction [21,26]. Copper is a feasible alloying element for liquid phase sintering. During the sintering process, copper melts and penetrates into the neck region between the bonded iron particles by capillarity action and subsequently diffuses into ferrite. It is noteworthy that the influence of copper is more pronounced in the presence of carbon [27]. In addition, phosphorus as a common alloying element can significantly affect the liquid phase

[1] QUCHAN UNIVERSITY OF TECHNOLOGY, FACULTY OF ENGINEERING, DEPARTMENT OF INDUSTRIAL ENGINEERING, QUCHAN, IRAN
[2] QUCHAN UNIVERSITY OF TECHNOLOGY, ENGINEERING FACULTY, DEPARTMENT OF MECHANICAL ENGINEERING, QUCHAN, IRAN
[3] RESEARCH AND DEVELOPMENT (R&D) MANAGER, MASHHAD POWDER METALLURGY, MASHHAD, IRAN

* Corresponding author: h.sazegaran@qiet.ac.ir

formation (during the sintering process) and microstructural and mechanical properties of the Fe-P-C steels [28].

In the sintered Fe-Mn-C low alloy steels, the addition of manganese causes to improve the mechanical properties [29]. The formation of Mn-oxide inclusions in sintered neck regions decreases the mechanical properties [30]. In the sintered Mn-Si steels, the formation of Mn-Si oxide inclusions depends on the sintering conditions [31]. Nickel can slightly decrease the temperature of liquid formation and increase the phase fraction of liquid [21,32]. Addition of carbon and molybdenum to Fe-Ni sintered alloys improves the distribution of nickel and forms a strong interaction between nickel and copper [33]. Addition of aluminum to the PM steels changes the microstructure and forms a stable AlN [34]. The addition of titanium in the microalloyed steels limits the grain growth during the sintering and increase the strength through precipitation hardening or solid solution strengthening [35]. Although numerous papers have been devoted to study the effect of various alloying elements on the PM steels, the effect of aluminum was rarely investigated. In this present work, the influence of aluminum contents (0, 2, 4, and 6 wt. %) on the porosity, microstructure and mechanical properties of Fe-C-Al sintered alloys was studied.

2. Materials and Experimental Methods

2.1. Materials

The commercial iron and aluminum powders produced by water atomization process were supplied from Mashhad Powder Metallurgy Company. The Fe-C-Al powder mixtures with composition of 0.5 wt. % C (pure, in the form of natural UF4 graphite, ash content below 0.1 wt. %) and addition of 0, 2, 4, and 6 wt. % Al were used. The purity, particle size distribution, and SEM micrographs of iron and aluminum powders are presented in Table 1 and Fig. 1, respectively. It can be seen from Fig. 1 that the shapes of the iron and aluminum particles are angular-irregular and rounded-irregular, respectively.

TABLE 1

Purity and distribution of particles

Powder type	Purity (%)	Particle size distribution (μm)		
		100-160	63-100	<63
Fe	99.9	18 wt. %	34 wt. %	48 wt. %
Al	99.9	23 wt. %	27 wt. %	50 wt. %

2.2. Manufacturing Process

To manufacture the PM steel specimens containing various amounts of aluminum (0, 2, 4, and 6 wt. %), the powder metallurgy technique was selected. Mixing process was performed using a rotary V-mixer machine (Rikon Pharma) at 200 rpm for 30 min. Based on the various amounts of aluminum (from 0 to 6 wt. %), four different types of mixtures were prepared. As lubricant, 0.3 wt. % of paraffin wax (Mashhad Powder Metallurgy Company, Iran) was added to the mixture. The green specimens were fabricated using a hydraulic press machine equipped with the cylindrical stainless steel die with an inner diameter of 12 mm and height of 200 mm. The upper and lower punches were manufacture of tool steel. The applied pressure was 650 MPa and the specimens were produced at an approximate height of 20 mm. By using double pressing, a nearly uniform densification of the green compacts is achieved. Finally, using a continuous tubular furnace, the sintering process was carried out at 1120°C for 52 min. The furnace atmosphere contained a mixture of nitrogen and hydrogen with the 90/10 ratio and the dewpoint was approximately 2°C. The main operations performed in the furnace for manufacturing of the PM steel specimens were dewaxing, sintering and water-cooling.

2.3. Density and Porosity

The green and as-sintered densities were calculated using Eq. (1). The porosity percentage was determined from sintered density using Eq. (2).

$$\rho = m/v \tag{1}$$

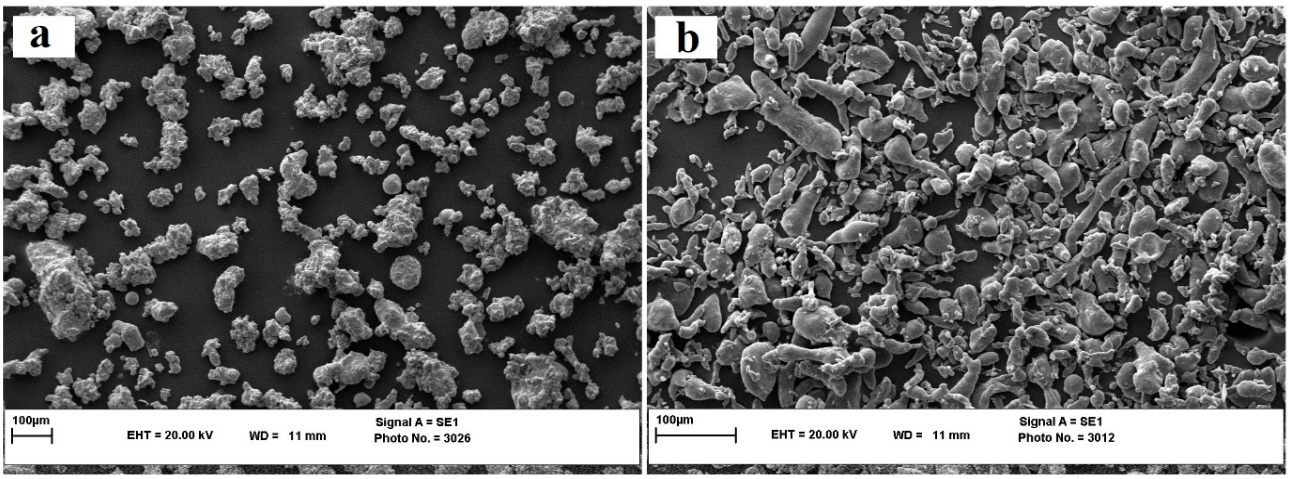

Fig. 1. SEM micrographs of a) Fe and b) Al powders

$$P_{Sintered} = \left[1 - \left(\frac{\rho_{Sintered}}{\rho_T}\right)\right] \times 100 \quad (2)$$

where: ρ, m, and v are density [g/cm^3], mass [g], and volume [cm^3], respectively and $P_{Sintered}$ is the porosity percentage of as-sintered specimens, $P_{Sintered}$ and ρ_T are density of the sintered steel (or apparent density) and theoretical density of the steel, respectively.

2.4. Microstructural Analysis

For microstructural observations, the PM steel specimens were cut using a wire-cut machine (Tops CNC, Model No. DK 7740, China). Then, the specimens were mounted, ground and polished in accordance with standard metallographic procedures (ASTM E3-11) followed by etching 2 vol. % Nital. The pore morphology and the microstructure of sintered steel specimens containing various amounts of aluminum were investigated using a light microscope (LM) equipped with the MIP^{TM} microstructural image processing software and a scanning electron microscope (SEM: LEO 1450VP). Prior to conducting the SEM studies, the specimens were coated with an Au-Pd alloy using a sputter coater machine (SC7620).

2.5. Mechanical Properties

In order to study the influence of aluminum contents on the mechanical properties of the sintered steel specimens, the Vickers hardness and compression tests were conducted. A Vickers hardness tester (HVS-50) was used to measure the values of the hardness of the cross-sectional sintered specimens. The hardness values represented for each specimen are average of at least five measurements. The compression tests were carried out according to ASTM E9 standard using a Zwick machine (Z250) with the cross speed of 0.5 mm/min. at room temperature [36]. The compression specimens were cut with the wire-cut machine from the sintered steels (length of 18 mm and diameter of 12 mm).

3. Results and discussion

3.1. Green and sintered densities

The mechanical behavior of the PM steels is affected by density and porosity, what has been confirmed in [37-41]. The green and sintered densities of steel specimens with different amounts of aluminum are shown in Fig. 2. The green and sintered densities differ from 7.17 to 7.31 g/cm^3 and 7.21 to 7.40 g/cm^3, respectively. By increasing the amount of aluminum, the green density decreases, due to the lower aluminum density (2.702 g/cm^3) in comparison with iron density (7.874 g/cm^3). In addition, the sintered density decreases with an increase in the amount of aluminum due to atomic diffusion that conducts the pores toward the surface of the sintered specimens [42]. In these sintering conditions, a liquid phase forms between the iron particles at an early stage of the process. Then, the molten metal penetrates along the iron grain boundaries and the densification is completed in a solid state.

Due to higher sintered density in comparison with the green density, it was found that the addition of aluminum to the powder mixtures affected the sintering process and causes a slight shrinkage. In contrast, dilatometric investigations of the sintering behavior of Fe and Al powders have shown that the formation of FeAl is accompanied by expansion due to volume change during the formation of the intermetallic phase Fe_2Al_5 [43]. In the specimens containing 0, 2, 4, and 6 wt. % of aluminum, differences between the green density and sintered density are 0.09, 0.07, 0.06, and 0.04 g/cm^3, respectively. This reduction in the differences, while the aluminum content increases, can be related to the improvement of aluminum diffusion by increasing the amount of aluminum [44]. It has been shown that the type of sintering process affects the density and porosity. Because of fast material transport via the liquid phase, the changes of pore morphology and porosity content during the liquid phase sintering are very fast. It can also be valid in a system with a very small volume fraction of liquid so that the liquid (even transient) is present only in the neck region between iron particles and the growth of particles is suppressed. The mechanism of pore filling is justified for most of liquid phase sintering where the grain shape can be considered to maintain an equilibrium shape. During manufacturing of porous Fe-C-Al alloys with high porosity, controlling the density (which depends on the porosity percentage and pore morphology) by the conventional powder metallurgy technique is much easier than the advance powder metallurgy methods (such as: electric current-assisted sintering, spark plasma sintering, and reactive synthesis) [45,46].

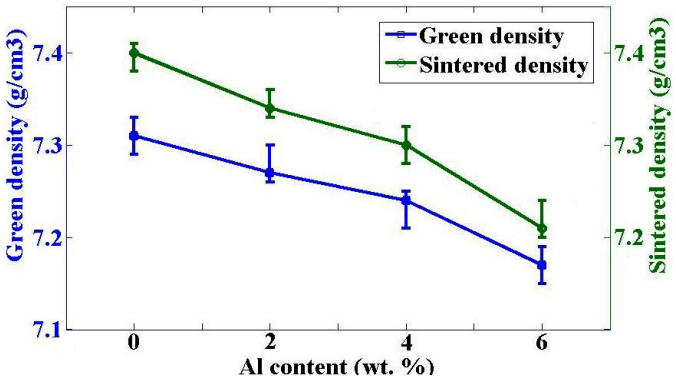

Fig. 2. The effect of aluminum content on the green and sintered densities of PM steel specimens

3.2. Porosity and pore morphology

The porosity percentage of sintered steels is shown in Fig. 3. The porosity percentage (Fig. 3) increases from 6 to 8.5% by increasing the amount of aluminum from 0 to 6 wt. %. It has

been reported that the porosity content of the PM steels depends on the size, shape and distribution of iron particles, alloying elements, lubricant agent, applied pressure, temperature, time and the sintering atmosphere, and is usually in the range of 5 to 15% [47,48]. Fig. 4 shows the LM and SEM images of pore distribution in the microstructure of steel containing 4 wt. % Al. The pores formed between the agglomerated iron particles are uniformly distributed in the matrix and have irregular and rounded shapes. Increasing the pressing pressure possibly reduce the pore size and porosity content [38]. In addition, the formation of pores between the sintered iron particles decreases the mechanical properties of PM steels [49].

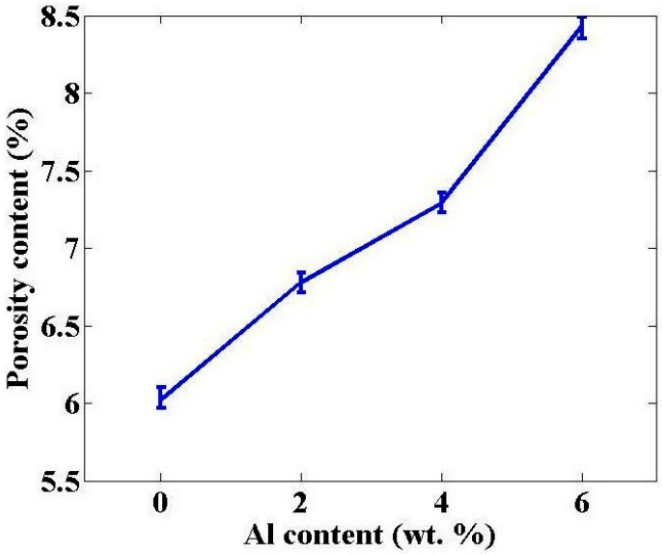

Fig. 3. The effect of aluminum content on the porosity percentage of steel specimens

3.3. Microstructure Investigations

The microstructures of Fe-0.5C-2Al specimen are shown in Fig. 5. In the sintering conditions (1120°C for 52 min.), the iron particles agglomerated together and the boundaries formed between the agglomerated iron particles. The microstructure of the PM steel specimens consists of ferrite and pearlite. In the pearlite, the formation of cementite layers between ferrite could be carried out because of diffusion of added carbon. The diffusion of carbon can significantly improve the formation of bonds between the agglomerated iron particles and thus, the me-

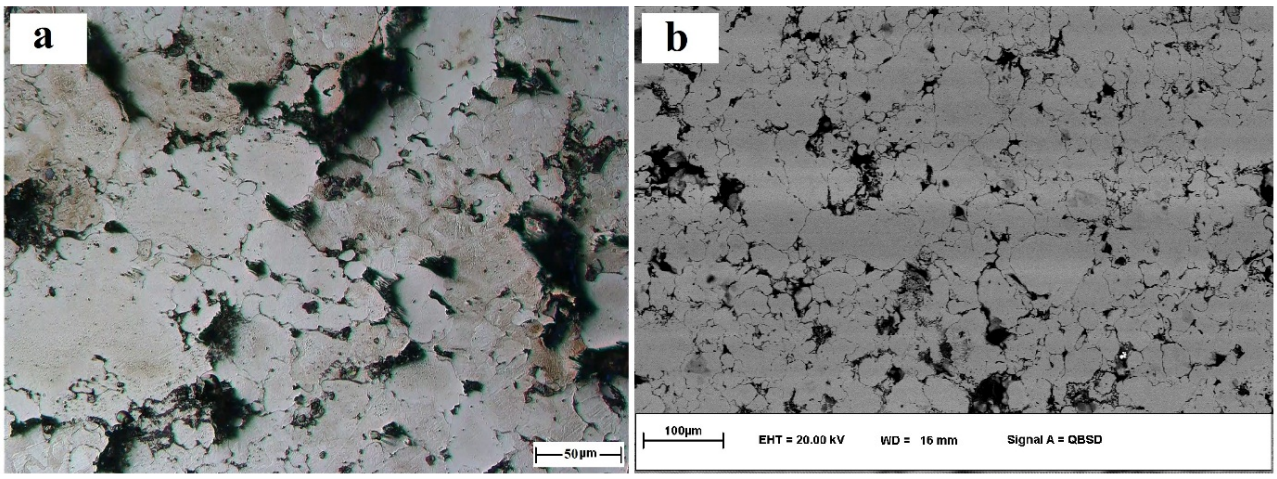

Fig. 4. a) LM and b) SEM porosity micrographs in the 4 wt. % Al specimen

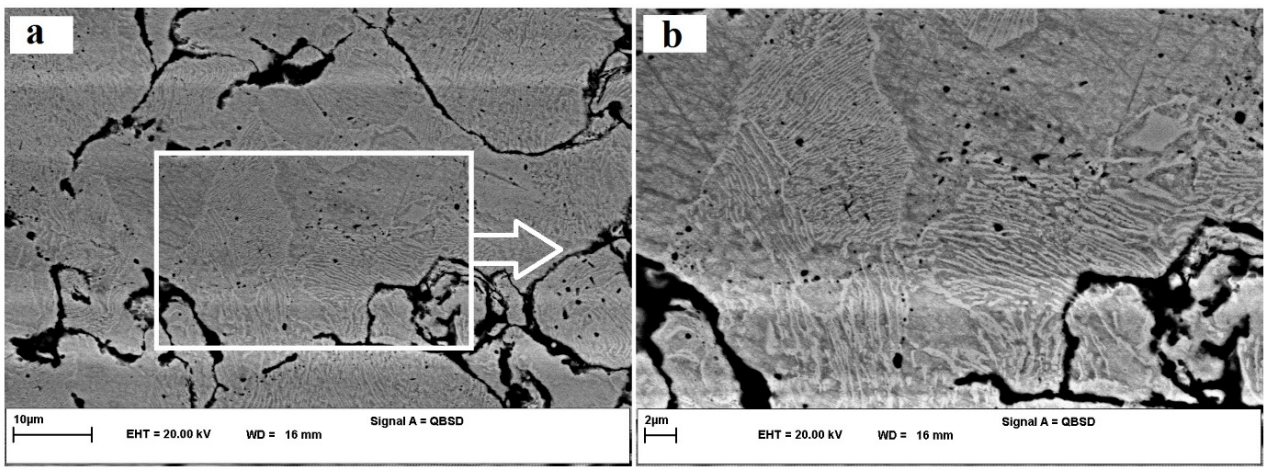

Fig. 5. The microstructure of the PM steel containing 2 wt. % Al (SEM)

chanical properties of PM steels enhanced [25]. At the sintering temperature (1120°C), aluminum oxide (alumina) likely forms on the surfaces of aluminum particles. In addition, aluminum nitride and iron aluminide form in the neck region between the agglomerated iron particles. The formation of polycrystalline layers on the surfaces of aluminum particles exposed to a nitrogen atmosphere have been reported. These layers consist of fine, rod-like crystallites of hexagonal AlN and double layers of AlN separated by a thin layer of aluminum which affect the mechanical behavior [50,51]. By analysis of the SEM images, the surface fractions of ferrite and pearlite were obtained 35.2 and 64.8%, respectively. It was found that the surface fractions of ferrite and pearlite did not depend on the aluminum contents.

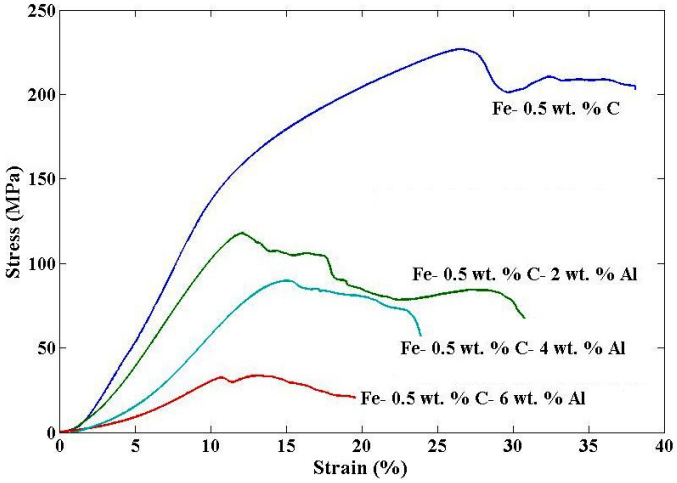

Fig. 6. The Stress-strain curves of PM Al-alloyed steels

3.4. Mechanical Properties

The mechanical properties of the PM iron alloys are influenced by the morphology of iron particles, alloying elements, lubricant agents, applied pressure, sintering conditions, density, porosity, and the microstructure [37]. By decreasing the density (increasing the porosity percentage) of sintered steels, the hardness, tensile, and fatigue characteristics decline [38,39]. Furthermore, increasing the porosity improves the friction and wear coefficients and sliding wear of sintered steels [14,40,41]. The stress-strain curves of steel specimens are shown in Fig. 6. Some similar behaviors are observed in all curves: elastic, plastic and strain softening regions. Some fluctuations of the stress were observed in the plastic region. This phenomenon is probably related to the pores connections and the growth of the cracks [30,52]. The pores formed between the agglomerated iron particles were the places of potential crack initiation and its propagation through the grain boundaries and matrix of PM steel [48].

The results illustrate that when the aluminum content is increased from 0 to 6 wt.%, the stress-strain curves shift downward. Some mechanical properties of steel specimens with different amounts of aluminum are shown in Fig. 7. It reveals

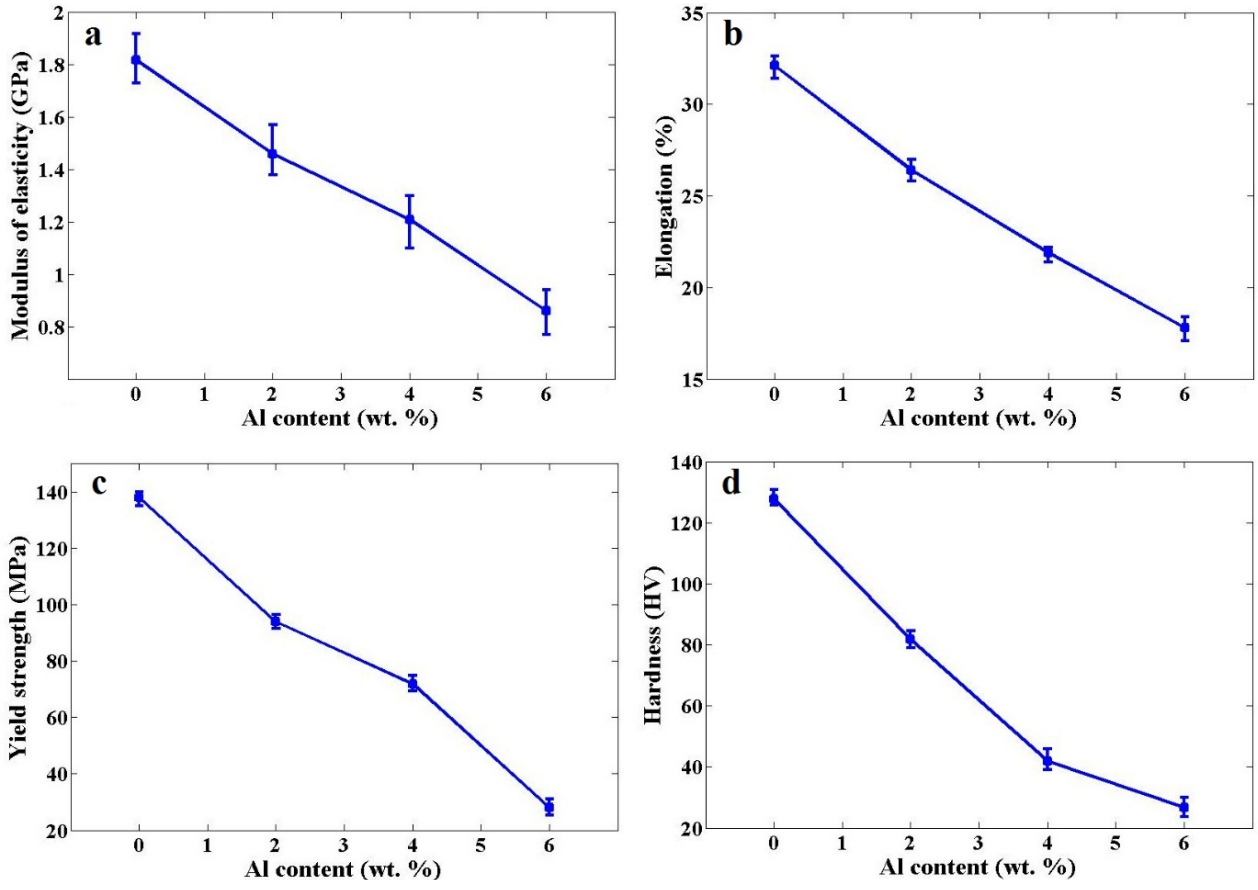

Fig. 7. The effect of aluminum content on the mechanical properties of investigated PM steels

that by increasing the amount of aluminum, the modulus of elasticity, elongation, yield strength, and hardness of the PM steel specimens are significantly reduced. During the transient liquid phase sintering process, the agglomerated iron particles bonds are weakened by formation of: molten aluminum, aluminum oxide on the surfaces of aluminum particles, aluminum nitride (due to the presence of nitrogen (10 vol. %) in the sintering atmosphere), and iron aluminide (or other intermetallic compounds). The weakened bonding results in a significant downfall of mechanical properties.

4. Conclusions

In this work, steel specimens containing (0-4) wt.-% Al and 0.5 wt.-% of carbon was successfully produced using powder metallurgy route. The effect of Al addition on the porosity percentage, microstructure, and mechanical properties was investigated. The results can be summarized as follows:

1 – The green and sintered densities of steel specimens decrease with increasing aluminum content.
2 – The higher sintering density compared to the green density indicates that shrinkage occurs during the sintering process.
3 – The porosity of investigated PM Al-alloyed steels increased with increasing Al content.
4 – The microstructure of PM steel specimens consists of ferrite and pearlite.
5 – As the amount of aluminum increases, the strain-stress curves of the investigated alloy steels shift downward, and the mechanical properties decline.

REFERENCES

[1] M.T. Andani, N. Shayesteh-Moghaddam, C. Haberland, D. Dean, M.J. Miller, M. Elahinia, Acta. Biomater. **10** (10), 4058-4070 (2014).
[2] P. Verma, R. Saha, D. Chaira, Powder. Technol. **326**, 159-167 (2018).
[3] J.M. Torralba, L. Fuentes-Pacheco, N. Garcia-Rodriguez, M. Campos, Adv. Powder. Technol. **24** (5), 813-817 (2013).
[4] C. Barile, C. Casavola, S.L. Campanelli, G. Renna, Eng. Fail. Anal. **95**, 273-282 (2019).
[5] S. Chauhan, V. Verma, U. Prakash, P. C. Tewari, D. Khanduja, T. Indian. I. Metals. **71** (1), 219-224 (2018).
[6] A. Garcia-Junceda, C. Diaz-Rivera, V. Gomez-Torralba, M. Rincon, M. Campos, J.M. Torralba, Mater. Sci. Eng. A. **740-741**, 410-419 (2019).
[7] L. Song-lin, H. Bai-yun, L. Yi-min, L. Shu-quan, L. Du-xin, F. Jin-lian, J. Feng, J. Cent. South. Univ. T. **10** (1), 1-6 (2003).
[8] P.K. Kumar, N.V. Sai, A.G. Krishna, Arab. J. Sci. Eng. **43** (9), 4659-4674 (2018).
[9] X. Yang, Y. Bai, M. Xu, S. Guo, J. Iron. Steel. Res. Int. **20** (7), 84-88 (2013).
[10] S. Decker, S. Martin, L. Kruger, Metall. Mater. Trans. A. **47** (1), 170-177 (2016).
[11] J. Park, S. Lee, S. Kang, J. Jeon, S. H. Lee, H. Kim, H. Choi, Powder. Technol. **284**, 459-466 (2015).
[12] K. Mahesh, S. Sankaran, P. Venugopal, J. Mater. Sci. Technol. **28** (12), 1085-1094 (2012).
[13] F. Martin, C. Garcia, Y. Blanco, Wear. **328-329**, 1-7 (2015).
[14] X. Li, U. Olofsson, Tribol. Int. **110**, 86-95 (2017).
[15] A. Falkowska, A. Seweryn, A. Tomczyk, Int. J. Fatigue. **111**, 161-176 (2018).
[16] F. Deirmina, M. Pellizzari, Mater. Sci. Eng. A. **743**, 349-360 (2019).
[17] W. Li, H. Xu, X. Sha, J. Meng, W. Wang, C. Kang, X. Zhang, Z. Wang, Fusion. Eng. Des. **137**, 71-78 (2018).
[18] O. Bergman, D. Chasoglou, M. Dahlstrom, Met. Powder. Rep. **73** (1), 21-25 (2018).
[19] T.K. Kandavel, R. Chandramouli, P. Karthikeyan, Mater. Des. **40**, 336-342 (2012).
[20] Y. Wu, R. M. German, D. Blaine, B. Marx, C. Schlaefer, J. Mater. Sci. **37** (17), 3573-3583 (2002).
[21] M.W. Wu, W.Z. Cai, Z.J. Lin, S.H. Chang, Mater. Des. **133**, 536-548 (2017).
[22] G.A. Baglyuk, L.A. Sosnovskii, V.I. Volfman, Powder. Metall. Met. Ceram. **50** (3-4), 189-193 (2011).
[23] S. Narayan, A. Rajeshkannan, J. Iron. Steel. Res. Int. **18** (9), 33-40 (2011).
[24] A.A. Nikulina, A.I. Smirnov, A.A. Bataev, A.S. Ivashutenko, Mater. Charact. **129**, 252-259 (2017).
[25] M.W. Wu, Metall. Mater. Trans. A. **46** (1), 467-475 (2015).
[26] M.W. Wu, Y.C. Fan, H.Y. Huang, W.Z. Cai, Metall. Mater. Trans. A. **46** (11), 5285-5295 (2015).
[27] T. K. Kandavel, R. Chandramouli, Int. J. Adv. Manuf. Technol. **50** (1-4), 53-59 (2010).
[28] W. Khraisat, L. Nyborg, Mater. Sci. Technol. **20** (6), 705-710 (2004).
[29] H. Chen, P. Luo, Y. Yang, A. Long, S. Li, J. Mater. Eng. Perform. **26** (9), 4481-4490 (2017).
[30] S. Gelinas, I. Bailon-Poujol, C. Blais, Mater. Sci. Eng. A. **730**, 391-400 (2018).
[31] R. Oro, E. Hryha, M. Campos, J.M. Torralba, Mater. Charact. **95**, 105-117 (2014).
[32] D.K. Behera, P. Tripathi, A.K. Chaubey, Mater. Today-Proc. **5** (1), 1704-1710 (2018).
[33] M. Nabeel, R. Frykholm, P. Hedstrom, Powder. Metall. **57** (2), 111-118 (2014).
[34] S. Haribabu, C. Sudha, S. Raju, R. N. Hajra, R. Mythili, J. Jayaraj, S. Murugesan, S. Saroja, Metall. Mater. Trans. A. **50** (3), 1-16 (2019).
[35] M.A. Erden, S. Gunduz, M. Turkmen, H. Karabulut, Mater. Sci. Eng A. **616**, 201-206 (2014).
[36] D. Firoozbakht, S.A. Sajjadi, H. Beygi, H. Sazegaran, Ceram. Int. **44** (15), 18156-18163 (2018).
[37] X. Deng, G.B. Piotrowski, J.J. Williams, N. Chawla, Int. J. Fatigue. **27**, 1233-1243 (2005).

[38] N. Kurgan, Mater. Des. **55**, 235-241 (2014).
[39] A. Falkowska, A. Seweryn, J. Szusta, Eng. Fract. Mech. **200**, 146-165 (2018).
[40] N. Chawla, X. Deng, Mater. Sci. Eng. A. **390** (1-2), 98-95 (2005).
[41] Y. Zhu, G. Lin, M.M. Khonsari, J. Zhang, H. Yang, J. Mater. Process. Technol. **262**, 41-52 (2018).
[42] Y.I. Kim, W. Lee, J.M. Jang, S.W. Ui, G.S. An, H. Kwon, S.C. Choi, S.H. Ko, J. Alloy. Compd. **747**, 211-216 (2018).
[43] S. Gedevanishvili, S.C. Deevi, Mater.Sci. Eng. A **325** (1-2), 163-176 (2002).
[44] R. Li, T. Yuan, X. Liu, J. Wang, H. Wu, F. Zeng, X. Zhou, T. Nonferr. Metal. Soc. **27**, 1594-1601 (2017).
[45] H.Y. Gao, Y.H. He, P.Z. Shen, Y. Jiang, C.T. Liu, Adv. Powder. Technol. **26**, 882-886 (2015).
[46] D.V. Dudina, B.B. Bokhonov, M.A. Legan, A.N. Novoselov, I.N. Skovorodin, N.V. Bulina, M.A. Esikov, V.I. Mali, Vacuum. **146**, 74-78 (2017).
[47] V.S. Warke, R.D. Sisson Jr., M.M. Makhlouf, Mater. Sci. Eng. A, **528** (10-11), 3533-3538 (2011).
[48] S. Gunduz, M.A. Erden, H. Karabulut, M. Turkmen, Powder. Metall. Met. Ceram. **55** (5-6), 277-287 (2016).
[49] M. Turkmen, Powder. Metall. Met. Ceram. **55** (3-4), 164-171 (2016).
[50] T. Pieczonka, T. Schubert, S. Baunack, B. Kieback, Mater. Sci. Eng. A **478** (1-2), 251-256 (2008).
[51] D. Kent, M. Qian, G.B. Schaffer, Powder. Metallurgy. **53** (2), 118-124 (2010).
[52] G. Straffelini, V. Fontanari, Eng. Fract. Mech. **78** (6), 1067-1076 (2011).